https://doi.org/10.5194/nhess-2020-2
Preprint. Discussion started: 16 March 2020

Natural Hazards and Earth System Sciences Discussions

1

Spatial and vertical structure of precipitating clouds and the role of background dynamics during extreme precipitation event as observed by C-band Polarimetric Doppler Weather Radar at Thumba (8.50^0N, 77.00^0E)

Kandula V Subrahmanyam and K. Kishore Kumar

Space Physics Laboratory, Vikram Sarabhai Space Centre, Thiruvananthapuram- 695022, India

E-mail: kvsm2k@gmail.com

Abstract

Extreme precipitation events have been cynosure for many meteorologists as well as for common men as it causes severe weather hazards and affects the densely populated regions, especially urban cities. It is now well known that these extreme events have been increasing over the Indian region during the past few years. It becomes very important to understand and assess these events, which is challenging in terms of limited observations. Very recently, the state of Kerala, India experienced extreme rainfall events during August 2018 and led to major flooding, which is regarded as one of the worst natural disasters experienced by Kerala in the last hundred years. This catastrophic event occurred during 12^{th} to 17^{th} August 2018 in which the Kerala state has received 60% more rainfall than the normal during this period. The present study focuses on investigating the spatial and vertical structure of precipitating clouds and their microphysical properties during this extreme precipitation event using C-band Polarimetric Doppler Weather Radar (DWR) observations over Thumba (8.50^0N, 77.00^0E). The DWR analyses were carried out during episodes of extreme rainfall, and the time evolution of radar reflectivity structure is examined very closely to understand the structure and dynamics of this unprecedented event. The spatial and vertical structures of precipitating clouds are strongly linked with the background dynamics. Apart from the DWR observations, prevailing dynamics such as tropical easterly jet (TEJ), low-level jet (LLJ) along with vertical velocity also investigated, which showed distant signatures lead to the extreme event. It was observed that the upper level divergence existed associated with low level convergence, which aids

https://doi.org/10.5194/nhess-2020-2
Preprint. Discussion started: 16 March 2020

Natural Hazards and Earth System Sciences
Discussions

to the development of convection. The westward equatorial waves were present in the period of 7-10 days throughout the month of August 2018. The weakening of TEJ at upper troposphere resulted in decrease of vertical shear, which favours the vertical growth of convective clouds leading to the extreme precipitation. The enhanced strength of LLJ is also contributed to the precipitation extreme. Thus, the significance of the present study lies in delineating the structure and dynamics of the extreme precipitation event using indigenously developed DWR.

Key words: Extreme precipitation, C-band DWR, Reflectivity, Zdr, TEJ, LLJ

1. Introduction

India is one of the densely populated countries in the world. Due to migrations of Inter Tropical Convergence zone (ITCZ) over the India, it experiences a strong seasonal variation in rainfall amounts. During summer i.e., June-September (winter i.e., December-February) months of India experiences large monsoon rains (dry period), where the ITCZ locates over the Indian subcontinent (Ocean) (e.g., Wang 2006; Ding 2007). The monsoon rains during the summer months provides the necessary water to the human needs as well as for societal benefits. The summer monsoon rainfall accounts for ~80% of annual precipitation over the Indian subcontinent which is crucial for the socioeconomic well-being and agriculture of billions of people in India (Ding and Sikka 2006; Alcide et al. 2019). But sometimes, it can also be associated with precipitation extremes and can impacts on the society of changing the hydrological cycle under warming climate. Even though, there have been may advances made in understanding the role of background dynamics, which cause extreme precipitation events and floods, but still they remain difficult predict.

Extreme precipitation events are increased in recent years and have drawn large attention across the globe to understand their causes (e.g., Del Genio and Kovari 2002; Fowler and Kilsby 2003;

https://doi.org/10.5194/nhess-2020-2
Preprint. Discussion started: 16 March 2020


Natural Hazards and Earth System Sciences Discussions

Alexander et al. 2006; Kerr 2013; Herring et al. 2014; Westra et al. 2013; Grosiman et al. 2013; Schumacher 2019). In the past studies debated that precipitation extremes increases with warming climate due to the larger amount of water vapour (Trenberth 1999; Allen and Ingram 2002; Pall et al. 2007; Muller et al. 2011). Precipitation extremes are vary under climate change and the increase in atmospheric moisture alone would able to happen precipitation extremes heavier at rate of $7\%K^{-1}$ (Held and Soden 2006; Sherwood et al. 2010). This increase in moister lead to the increase in latent heating which may lead to stronger vertical ascent and thus adding the additional amount of precipitation (Nie et al. 2018). The Indian summer monsoon also plays a significant role in climate variability and previous studies confirmed that there is an increase in the amount of water vapour over the Indian region (e.g., Mukhopadhya et al. 2017). This increase in water vapour is attributed to the increased occurrence of extreme rainfall events over the Indian region (e.g., Goswami et al. 2006; Soden and Held 2006; Rajeevan et al. 2008). Soden and Held (2006) attributed to the large variability in low-level monsoon jet over the Arabian Sea in recent years, which supply surplus moisture leading to the extreme precipitation events over the Indian subcontinent. Further, the tendency of deep convective activity is also caused for the increased water vapour in the atmosphere. It is found that the deep convective systems, whose life time is more than 6 hours have contributed 50% more water vapour in the mid-troposphere compared to short lived convective systems (Baisya et al. 2018; Derbyshire et al. 2004; Feng et al. 2012). IPCC (2002; 2007) report emphasized to understand the behavioural characteristics of extreme rainfall events and how background environment dynamics influences such events.

An extreme rainfall event influences the average rainfall over the region, ecosystems, land scale through erosion processes and leads to major floods (O'Gorman 2015). It also severely affects riverbeds and many houses were turfed by this event. Extreme precipitation events are increasing more rather than mean precipitation in regional as well as globe and they have significant variability across geographic locations (Alexander et al. 2006; Westra et al. 2013). Hurricane Katrina, which

https://doi.org/10.5194/nhess-2020-2
Preprint. Discussion started: 16 March 2020


Natural Hazards and Earth System Sciences Discussions

was one of the most deadly storms severely, damaged the Gulf cost of America in August 2005 and around 1800 people died (Houze et al. 2006). In 2010, a major heavy rainfall flood occurred in Pakistan and killed around 17000 people and millions of homes were damaged (Kirsch et al. 2012). Another major disaster happened in Canadian history in 2013 due to extreme precipitation events, which led to Alberta floods (Milrad et al. 2015). So there is great concern about these frequency and intensity of extreme precipitation events (Muller et al., 2011). There have been studies on extreme rainfall trend over India (e.g., Rajendra Kumar and Dash 2001; Goswami et al. 2006; Rajeevan et al. 2008; Ajayamohan et al. 2010; Krishnamurthy 2011) since 1998 and few of them are mentioned. The State of Assam in India suffered by severe flood in 1998 and it regularly grappling with them. In July 2005, Mumbai faced the very heavy rainfall, which lead to flood and killed over 700 people and some of the areas around the Mumbai were under water. The high intensity rainfall occurred in October 2009 was the one of the worst flood in India, which killed around 300 people and made 5 lakhs homeless. The Leh flood in August 2010, Utharkhand flood in 2013, heavy rain fall in 2014, Gujarat flood in 2017 and very recent Kerala flood in 2018 were severely damaged the property ad infrastructure and also took many of human life's. The extreme precipitation event occurred in Kerala in August 2018 was the highest rainfall in a century. This event was associated with unusually very high amount of rainfall during ISM and about 60 % more than the rainfall in Kerala contributed by this extreme precipitation rainfall during ISM period. The west coast of Kerala and Western Ghats receives a heavy rainfall during Indian summer monsoon region and it contributes significantly to the average rainfall (Rao 1976; Soma and Krishnakumar 1990; George 1956; Srinivasan et al. 1972; Mukherjee and Kumar 1976; Mukherjee et al. 1978; Mukherjee 1980). There have been studies on the heavy rainfall events, which the daily rainfall exceeding 15 cm over the west coast occur on many days cause extensive damage.

There have been numerous studies funnelled on numerical simulations of extreme precipitation events (e.g., Hennessey et al. 1997; Held and Soden 2006; Muller et al. 2007; Sherwood et al. 2010;

https://doi.org/10.5194/nhess-2020-2
Preprint. Discussion started: 16 March 2020


Natural Hazards and Earth System Sciences Discussions

106 Muller et al. 2011; Siler and Roe 2014; O'Gorman 2015; Shi and Durran 2015; Collow et al. 2016;
107 Nie et al. 2018; Tandon et al. 2018). Climate model studies showed that these extreme events
108 heavily depend on the region, where some regions experiences severe extremes, while other
109 experiences decrease in such events (e.g., Tandon et al. 2018). They also said that the drivers of
110 precipitation extremes are remains conundrum and poorly understood. Further, studies also showed
111 that changes in mean temperature and vertical velocity (e.g., Muller et al. 2011) and anomalous
112 moisture transport and lower sea level pressure (e.g., Collow et al. 2016) play a crucial role in
113 strength of such precipitation extremes. Orography also play a vital role in precipitation extremes
114 and there have studies on the understanding the orographic response to extreme precipitation events
115 in climate point of view (e.g., Nie et al. 2018; Muller et al. 2007; O'Gorman 2015; Shi and Durran
116 2015; Siler and Roe 2014; Held and Soden 2006; Sherwood et al. 2010). From their studies it found
117 that the occurrence of extreme precipitation events are more over lee-ward side compared to wind-
118 ward climatologically. This is mainly due to the downstream precipitation transport and cause the
119 large condensation increases, which leads to lee-ward precipitation (Siler and Roe 2014). In
120 addition, the changes in vertical velocity also found to be different during extreme precipitation
121 events and modify background thermodynamics (Shi and Durran 2015). Duration of these extreme
122 events impacts the amount of precipitation and also on society (Kao and Ganguly 2011). The short
123 bursts of extreme precipitation events might lead to an increase in total rainfall, but they do not
124 significantly contribute to groundwater discharge. Synoptic meteorological conditions are also led
125 to the development of precipitation extremes. There have been several research studies on the role
126 of synoptic scale influences on precipitation extremes over the globe (e.g., Catto et al. 2002;
127 Takahashi 2004; Catto and Pfahul 2013; Milrad et al. 2015; Agel et al. 2018). Catto et al. (2002)
128 studied daily rainfall over the globe and found that approximately 30-42% is related to warm fronts,
129 while 18-30% is related to cold fronts. However, the precipitation extremes are more likely to be
130 associated with warm fronts (e.g., Catto and Pfahul 2013). They found that the around 40-50%
131 extreme precipitation occurs nearby locations of warm fronts in the Northeast. Takahashi (2004)

https://doi.org/10.5194/nhess-2020-2
Preprint. Discussion started: 16 March 2020


Natural Hazards and Earth System Sciences Discussions

studied the precipitation extreme associated with atmospheric circulation in Peru during 2002. They suggested that heavy rainfall days are associated with the enhanced strength of low-level westerly, which helps the development of convection by orography lifting. Agel et al. (2018) examined the various meteorological parameters and found that there is large difference between the days with and without extreme events. Further, they attributed three dimensional structure of tropopause is one of the factor relevant to precipitation in terms of circulation along with other meteorological parameters in the north east of United States. Nonetheless, these extreme precipitation events are difficult to manage and have dire consequences on water resource, infrastructure and agriculture.

In the present study, we used C-band polarimetric Doppler Weather Radar (DWR) observations to characterize the spatial and vertical structure of precipitating clouds during extreme precipitation event on 15th August 2018. We also investigated the dynamical meteorological parameters responsible for the occurrence of precipitation extremes using Era-interim reanalysis data. Section 2 describes the measurements of C-band DWR and soundings at Trivandrum and Era-interim reanalysis also discussed. The temporal evolution of spatial and vertical structure of precipitating clouds is discussed in Section 3. Section 4 presents the changes in the background dynamics. The summary of the present study is summarized and concluding remarks were presented in section 5. The central objective this manuscript is to characterize the spatial and vertical distribution of reflectivity (Z), differential reflectivity (Zdr) and the role of large-scale circulation lead to the occurrence of extreme precipitation event.

2. Description of C-band polarimetric DWR and base products

C-band polarimetric DWR is installed at Thumba and is continuously operating for monitoring weather systems. This system was developed by Bharat Electronics Limited (BEL), Bangalore with technology provided by Indian Space Research Organisation (ISRO). This is the first polarimetric

https://doi.org/10.5194/nhess-2020-2
Preprint. Discussion started: 16 March 2020

Natural Hazards and Earth System Sciences Discussions

158 DWR installed in India along the western coast of India. Figure 1 (a) & (b) shows geo-location of
159 the C-band polarimetric DWR at Thumba and its building and radome of DWR can be seen. The
160 volume coverage pattern of C-band DWR is shown in figure 1(c). The elevation angles are 0.5^0, 1^0,
161 2^0, 3^0, 4^0, 7^0, 9^0, 12^0, 15^0, 18^0 and 21^0 steps. Total 11 elevation steps are considered for full volume
162 scan. The major specification of C-band DWR is provided in Table 1. The central operating
163 frequency of DWR is 5.625 GHz and the antenna rotation is 0.5 to 6 rpm (rotation per minute). The
164 gain of the antenna is 45 dB. The transmitter is Klystron and the peak power is 250 kW. The pulse
165 widths are selectable from 0.5, 1, 2, 3 and 4 μs. The antenna sweeps 360 degrees in azimuth and 11
166 steps in elevation as mentioned above. For the present study, we have used C-band DWR
167 observations during extreme precipitation event during 12^{th} to 18^{th} August 2018. During that time,
168 C-band DWR is operated round the clock and provided valuable information on three-dimensional
169 structure of precipitating clouds in extreme precipitation. The scan strategy employed in DWR as
170 given follows: 1. Single PRF (Pulse Repetition Frequency) - 400 Hz with 3 elevation steps; pulse
171 width is 2 μs; scan RPM (rotation per minute) is 1.5; DTP (dwell time pulses) is 44 and the range
172 resolution is 300 meters. 2. Dual PRF - 450/600 Hz with 11 elevations; pulse width is 1 μs; scan
173 RPM is 1.5; DTP is 57 and the range resolution is 150 meters as mentioned in Table 1. For the
174 present analysis, we utilized the dual PRF observations only, where the DTP is high and provides
175 the full volume scan. Single PRF scan takes around ~ 6 minute to complete full volume san with
176 three elevations, while dual PRF scan takes around ~ 8-9 minutes. Therefore, the dual PRF volume
177 scans are available with ~15 minutes interval time. So, there are totally ~ 8 to 9 volume scans
178 available in each hour. The radar data is stored in polar co-ordinates (i.e., in terms of range, azimuth
179 and elevation). For the present analysis, the radar data on the polar coordinates have been converted
180 into Cartesian coordinates.

181
182
183
184
185

https://doi.org/10.5194/nhess-2020-2
Preprint. Discussion started: 16 March 2020

Natural Hazards and Earth System Sciences
Discussions

Table 1: Specifications of C-band DWR at Thumba

Major Technical specifications	
Operating frequency	5.6 – 5.65 GHz
Polarization	Single and Dual polarizations
Antenna rotation	0.5 to 6 rpm
Antenna Gain (dB)	45
Radome survival wind speed	200 $kmhr^{-1}$ steady
Transmitter	Klystron
Transmitter peak power	250 kW
Pulse width	0.5, 1, 2, 3, 4 µs
Elevation levels (degree)	0.5, 1, 2, 3, 4, 7, 9, 12, 15, 18, 21
Azimuth sweeps (degree)	0-359

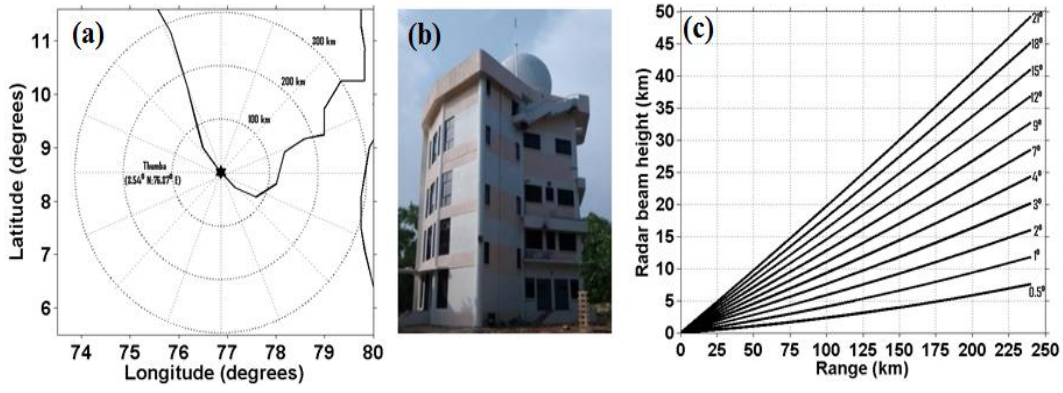

Figure 1: Geolocation of the C-band polarimetric DWR building at Thumba and radome of DWR and the volume coverage pattern

Figure 2 (a-c) shows the base products of plan position indicator (PPI) of reflectivity (Z), Doppler velocity (v) and spectrum width (sigma) on 15th August 2018 at 07:51 UT at 3 degree elevation. Each solid black circle represents the 50 km range from the radar centre as shown in figure 2. From this picture, it is clearly seen that the precipitating system was widely covered in the radar range and the direction of cloud system in south-westerly as the prevailing wind is south-westerly during the monsoon months. The maximum precipitating cloud system was concentrated in between 50 to 100

https://doi.org/10.5194/nhess-2020-2
Preprint. Discussion started: 16 March 2020

Natural Hazards and Earth System Sciences
Discussions

216 km from the radar range. The higher the reflectivity values associated with the larger rainfall
217 regions. The maximum reflectivity observed at this time was around 40 dBZ. The corresponding
218 radial velocity was shown in Figure 2(b). Radial velocity information is very useful for identifying
219 the change of wind with space and time. Negative (Positive) values corresponds to precipitating
220 cloud system is approaching towards (away) the radar. This can be clearly seen in Figure 2(b),
221 where blue (red) colour indicates the systems moving towards (away) the radar centre. Often the
222 change in wind is gradual, but it can be quite sudden in the cases of complex convective systems.
223 Even, a quite sudden wind change is observed during this extreme precipitation event in Figure 1(b)
224 indicated by red colour circle. It supposed to be negative because system is moving towards the
225

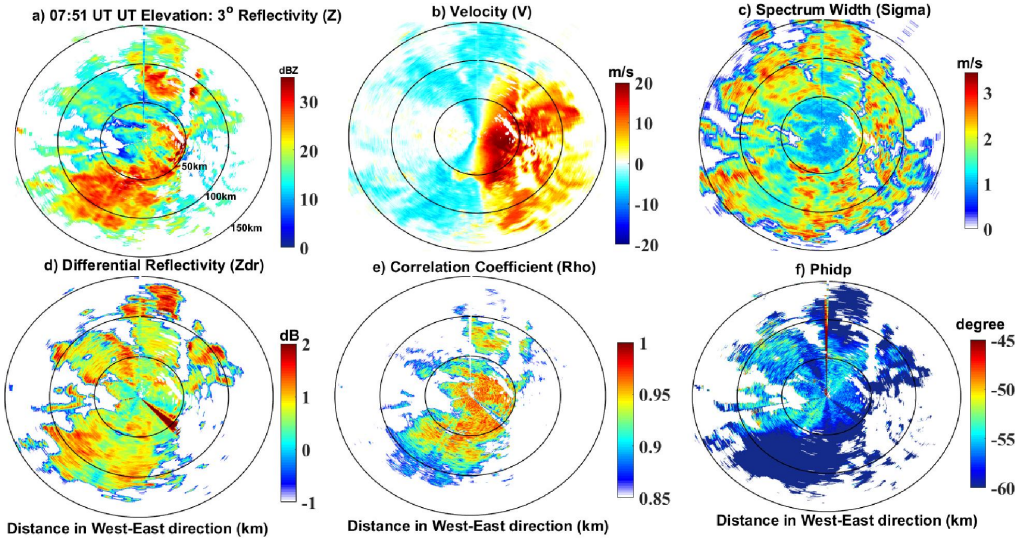

226

227 *Figure 2: C-band DWR base products (a-c): reflectivity, velocity and spectrum width; polarimetric*
228 *products (e-f): differential reflectivity, correlation coefficient and differential phase shift*
229 *respectively at 07:51 UT on 15th August 2018*
230
231
232 radar, but rather it is positive, which suggests that there is presence of off shore convective vortices
233 occurred just south of the radar location (Rao, 1976), which embedded in the extreme precipitating
234 system. It is also evident in Figure 2(c) of DWR spectral width where the large values of spectral

https://doi.org/10.5194/nhess-2020-2
Preprint. Discussion started: 16 March 2020


Natural Hazards and Earth System Sciences Discussions

235 width observed. Spectral width is the measure of turbulent in precipitating systems. Figure 2(d-f)
236 shows the polartimetric products of differential radar reflectivity (Z_{dr}), cross correlation coefficient
237 (ρ_{hv}) and differential phase shit (ϕ_{dp}) respectively. The Z_{dr} gives the ratio between the horizontal
238 reflectivity and vertical measured reflectivity. The maximum Z_{dr} is found to be between 1 and 1.5
239 dB, which suggest that the hydrometeors are oriented in horizontal direction and oblate (Figure
240 2(d)). Negative Z_{dr} represents the hydrometeors which are oriented vertical direction. Zero Z_{dr}
241 corresponds to the hydrometeors are circular in shape. Therefore we can identify the orientation of
242 the hydrometeors by inspecting distribution of Z_{dr}. It is evident from figure 2(d), that these echoes
243 mainly meteorological (Figure 2(e)) as the ρ_{hv} values are 0.9 and above and are homogeneous. The
244 other polarimetric quantity is ϕ_{dp} is the difference between the phases of the copolar signal at
245 horizontal polarization (ϕ_{hh}) that at the vertical polarization (ϕ_{vv}). Around 5-10 degree phase delay
246 is observed during this time and this is mainly arises due to the hydrometeors in the convective
247 cloud systems. Since ϕ_{dp} is independent on radar parameters, it is very useful quantity for
248 calibrating the radar.
249
250 **3. Results and Discussions**
251 **3.1 Temporal evolution of spatial and vertical structure of reflectivity**
252
253 Figure 3 shows the temporal evolution of spatial structure of reflectivity at 3 degree elevation from
254 04:30 UT to 08:00 UT with a time interval of 30 minutes on 15th August 2018. This picture reveals
255 that precipitation occurred over almost entire radar coverage. The development of precipitating
256 systems is clearly depicted in this figure. With time progress, enhancement of convection was
257 observed right from 04:30 UT to 07:51 UT in intensity as well as spatial pattern (Figure 3). The
258 movement of convective precipitation band is south-westerly. The maximum reflectivity is found to
259 be north of the radar at 04:30, 05:03 and 05:33 UT times, which is associated with deep convection,

https://doi.org/10.5194/nhess-2020-2
Preprint. Discussion started: 16 March 2020

Natural Hazards and Earth System Sciences
Discussions

where it was located over the Arabian Sea. It then became weak, when it moved over land at 06:04 UT and at the same times another convective system present over the ocean (south-west direction). In addition, a distinct narrow rain band oriented along south-north direction with enhanced reflectivity developed at 05:03 UT. Further, it widened as time progresses and intensified as seen in Figure 3(e, f, & g). This narrow band with high reflectivity is called as monsoon warm fontal system, which embedded in the extreme precipitating system and it indicated by black solid line in Figure 3. The embedded monsoon frontal system enhanced with time and caused for the extreme rainfall observed on 15th August 2018. Catto and Pfahul (2013) observed similar kind of precipitation extreme associated with frontal systems. The precipitating system was fully covered over the radar range by 07:51 UT. This is the time, where the most of places in and around Kerala got heavy rainfall and it is strongly linked to the low-level westerly. During this time, the LLJ became intensified and persisted throughout the extreme period which triggered the heavy precipitation. Further, TEJ and vertical velocities also played vital role in enhancements of extreme precipitation, which will be discussed in next section.

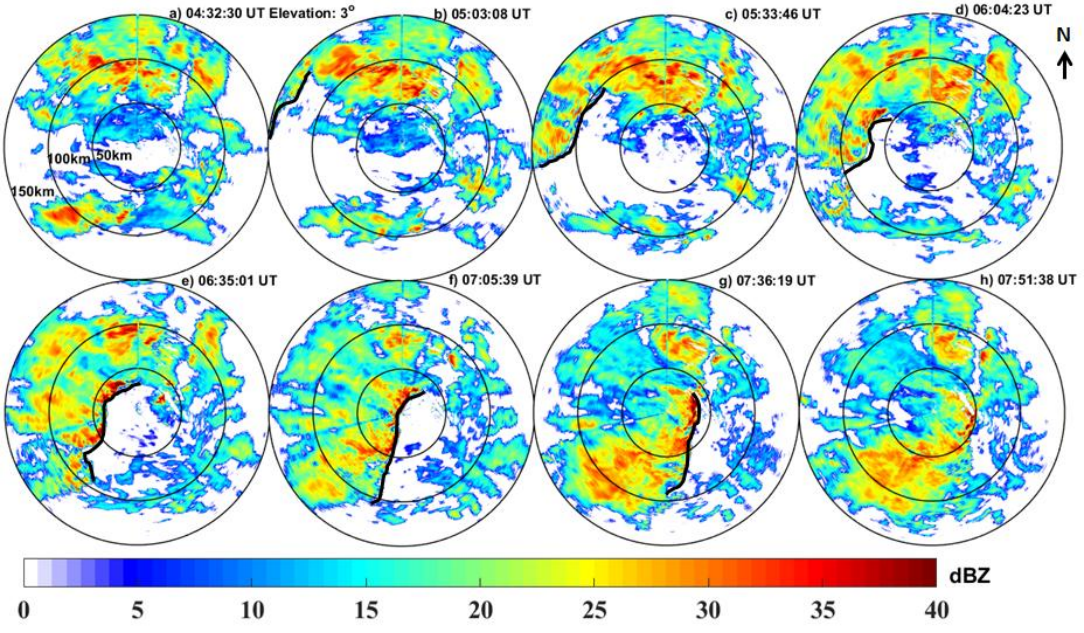

https://doi.org/10.5194/nhess-2020-2
Preprint. Discussion started: 16 March 2020

Natural Hazards and Earth System Sciences
Discussions

Figure 3: (a-h): Temporal evolution of spatial structure of reflectivity at around 30 min. time interval from 04:30 UT to 08:00 UT at 3 degree elevation on 15th August 2018: Black solid line indicates the progresses of monsoon frontal systems.

The precipitating cloud tops are observed to be around 10 km, which is associated with frontal convective system as seen in Figure 4. Figure 4 shows the vertical cross sections of radar reflectivity along frontal convective system at (a) 05:33 UT and (b) 06:35 UT. During its early development stage, the observed precipitating cloud top is around 6 km and the convective core width is to be around 3km (Figure 4(a)). At this time, there are multiple shallow convective cells behind the leading convection, which are embedded in the frontal systems. Further with rapid intensification, the precipitating cloud tops are reached beyond 10 km, where the strong updraft prevails. And the convective core width is to be 7 km (Figure 4(b)). The maximum reflectivity is found to be about 45 dBZ. The multiple convective cells merge and became single convective cell. A zone of cloud free was observed immediately after the leading convective core. This is mainly due to the descending motion associated with convective updrafts, which subsidises the cloud development as seen Figure 4.

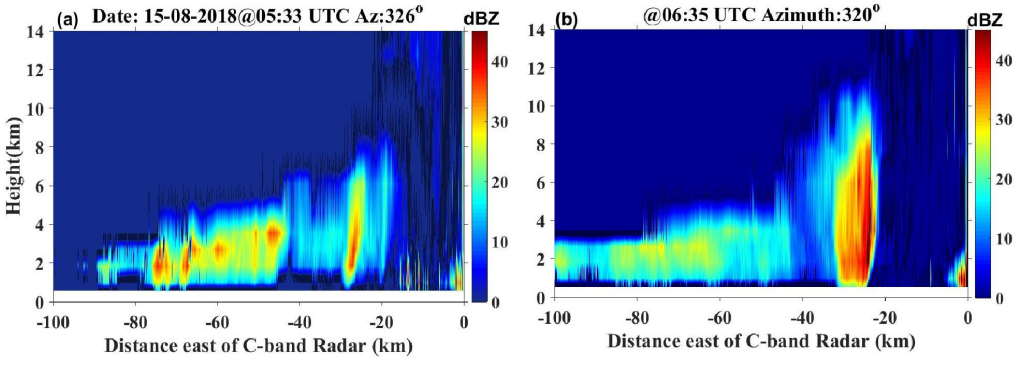

Figure 4(a-b): Vertical cross sections of radar reflectivity along frontal convection at 05:33 and 06:35 UT.

Further to study the temporal evolution of vertical profiles, time series of vertical structure of reflectivity is plotted in Figure 5. Figure 5 shows the temporal distribution of vertical structure of reflectivity at various development stages during extreme precipitation on 15th August 2018. At time

https://doi.org/10.5194/nhess-2020-2
Preprint. Discussion started: 16 March 2020

Natural Hazards and Earth System Sciences
Discussions
Open Access
EGU

298 04:32 UT, the convective precipitating system was developed at around 20 km from the radar centre
299 in north-west direction as shown in Figure 5(a). With time progresses (04:32-06:05 UT), the system
300 was then became more vigorous with taller cumulus congests cloud with high reflectivity values
301 (Figure 5(b-c)).The deepest cloud observed at this time, where the higher reflectivity values are
302 concentrated in narrow band at 15 km west to the radar centre (Figure 5(c)). During that time
303 (06:05-07:05 UT), multi convective cells embedded in the extreme precipitation were observed with
304 broader reflectivity band as seen in Figure 5 (d-e).
305

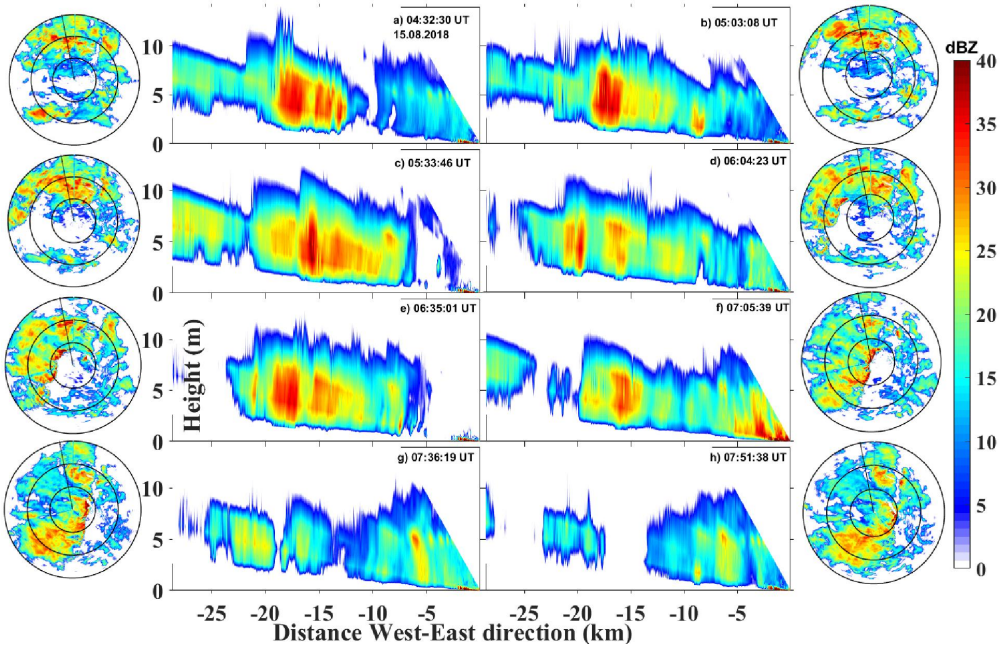

306

307 *Figure 5 (a-h): Vertical cross sections of radar reflectivity. Corresponding cross sections were also*
308 *shown*.
309

310 Figure 6 shows the Hovmöller diagram of (a) maximum reflectivity and (b) maximum differential
311 reflectivity on 15th August 2018 within the radar range of 80 km. Red boxes indicate the episodes of
312 first and second intense rainfall. From this picture, it is clearly evident that the rainfall occurred in
313 three spells (Figure 6(a)). The first spell was occurred during 04 UT to 08 UT, where the radar
314 rainfall continuously observed. And after four hours, second spell of continues rainfall occurred

https://doi.org/10.5194/nhess-2020-2
Preprint. Discussion started: 16 March 2020

Natural Hazards and Earth System Sciences
Discussions
Open Access
EGU

315 from ~12 UT to 16 UT. The time duration of the third spell was less than hour. During the first spell
316 of extreme event, widespread rainfall with maximum Z were observed, which shows that there were
317 embedded convective cells with the extreme precipitation. These convective cells were eastward
318 propagation as clearly evident in Figure 6. Therefore, the time series of maximum reflectivity
319 reveals that the extreme precipitation event was not in continuous rather bursts of heavy
320 precipitation, which caused to receive the large amount of rainfall in a short time, resulting in a high
321 runoff rather than groundwater charging and subsequently led to observed flood over Kerala in
322 August 2018 (Mishra et al., 2018). Immediately, water levels in rivers and reservoirs have received

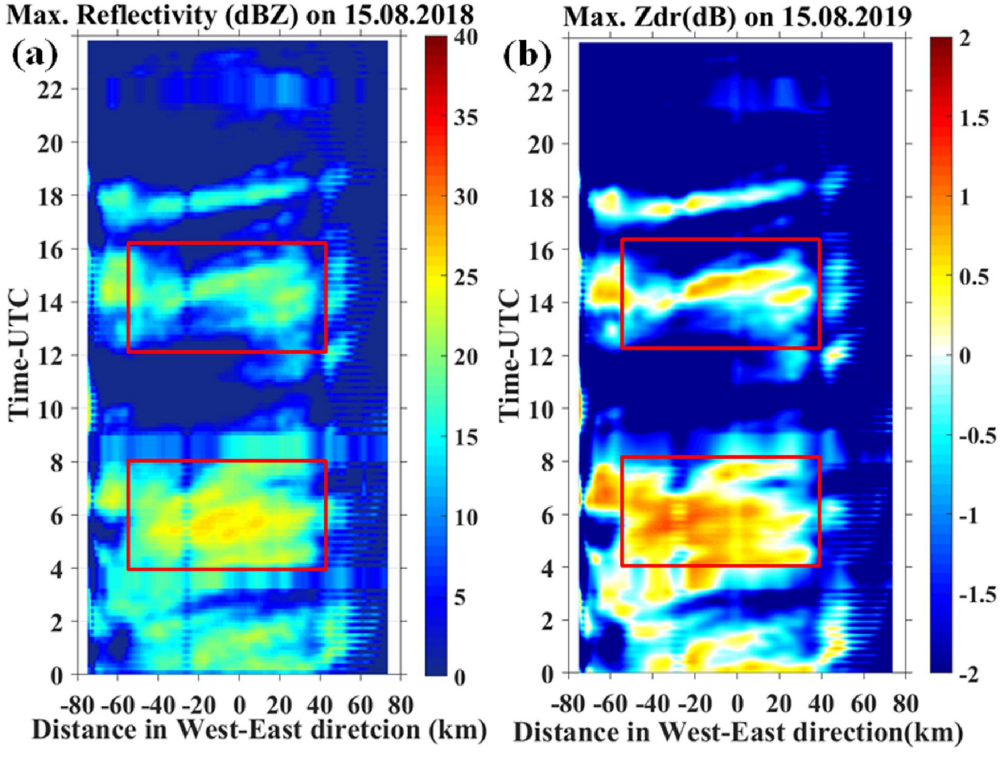

323

324 *Figure 6: Hovmöller diagram of (a) maximum reflectivity and (b) maximum differential reflectivity.*
325 *Red boxes indicate the episodes of intense rainfall.*
326

327 the record level of inflow. Since the DWR has the capability of polarimetry, the temporal evolution
328 of maximum Z_{dr} shown in Figure 6(b). This provided vital information on the microphysical nature
329 of hydrometeor during extreme precipitation event. There were many studies using DWR

https://doi.org/10.5194/nhess-2020-2
Preprint. Discussion started: 16 March 2020

Natural Hazards and Earth System Sciences
Discussions

observations during extreme precipitation, but very less on polarimetric observations, especially in India. The highest maximum Z_{dr} found to be 0.8 to 1 dB, which suggests that the most of the hydrometeor particles are oriented in horizontal with respect to radar beam and oblate in nature. The maximum Z of ~ 18 dBZ and less value were associated with negative Z_{dr}, which indicates that particle in vertically oriented (Figure 6). Figure 7 shows the DWR derived rainfall accumulation on (a) 12th (b) 13th (c) 14th and (d) 15th August 2018. The maximum rainfall occurred during extreme precipitation is around 300 mm and more from 12th to 5th August 2018, which led to heavy flood in Kerala (Figure 7(d)).

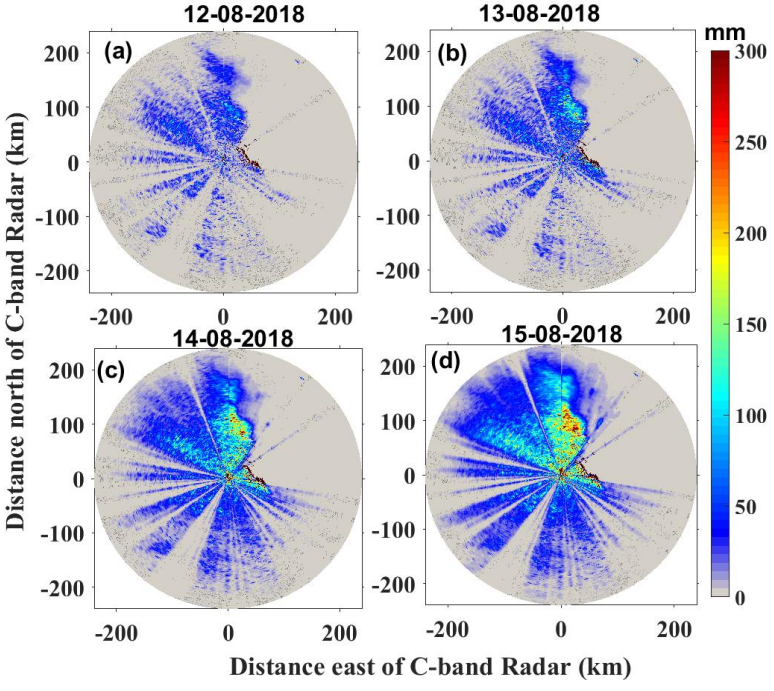

Figure 7: Rainfall accumulation derived from C-band DWR on (a) 12th (b) 13th (c) 14th and (d) 15th August 2018.

3.2 Role of background dynamics for the observed extreme precipitation event

In this section, we looked into the changes in the background dynamic caused for the observed extreme precipitation in Kerala during August 2018. There should be pre-existence needed for

https://doi.org/10.5194/nhess-2020-2
Preprint. Discussion started: 16 March 2020

Natural Hazards and Earth System Sciences
Discussions
Open Access
EGU

346 severe convective system to occur, which includes a high amount of convective available potential
347 energy (CAPE), steady supply of moisture, wind shear and low-level convergences. The Indian
348 monsoon is characterized by moist convective instability with relatively high amount of CAPE
349 (Xavier et al. 2018). Figure 8 shows that the daily variation of CAPE, which suggest that prior to
350 occurrence of extreme precipitation, large CAPE values observed and helps to the initiate the
351 vigorous convection during extreme precipitation. It is also noticed from Figure 8, that the
352 maximum CAPE value observed just three days priors to the day of extreme precipitation. Recently,
353 Xavier et al. (2018) observed the similar changes of CAPE during the Uttarakhand heavy rainfall

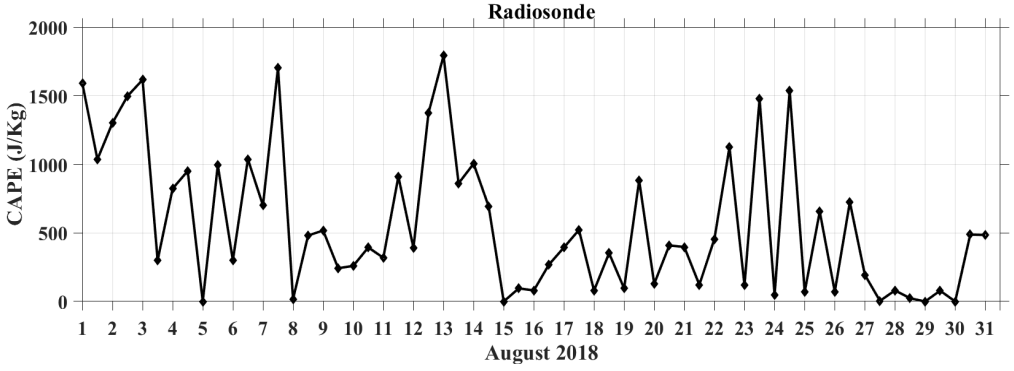

354

355 *Figure 8: Day-to-day variability of CAPE derived from radiosonde observations at Trivandrum*
356 *during August 2018.*
357

358 event in June 2013. We have carried analysis for three periods such as before (1st -7th August),
359 during (12th -18th August) and after (25th -31st August) the extreme precipitation event as shown
360 figures 9 & 10 for LLJ and TEJ. The Indian summer monsoon months has the strong south-westerly
361 wind, which carries the moisture-laden from the Arabian Sea. The supply of moisture depends on
362 the strength of the LLJ and orographic lifting happens when LLJ encounter Western Ghats (e.g.,
363 Sarker 1964). In addition, Western Ghats are also capable of producing the offshore convection and
364 initiate the convection due to orographic lifting (e.g., Grossman and Durran 1984; Smith 1985).
365 Further, to investigate the large-scale circulation, we have examined the LLJ at 850 hPa, TEJ at 150
366 hPa using ERA-interim reanalysis data, where the maximum zonal wind strength observed during
367 August 2018. In the present study, the strength of the LLJ is more during the event (Figure 9(b))

https://doi.org/10.5194/nhess-2020-2
Preprint. Discussion started: 16 March 2020

Natural Hazards and Earth System Sciences
Discussions
Open Access
EGU

368 compared to before (Figure 9(a)) and after the event (Figure 9(c)). Interestingly, LLJ has single
369 branch during extreme event time, while it has two branches (one over the Indian continent and
370 other over the Srilanka) as expected in normal conditions. The enhanced moisture supply by LLJ
371 from the Arabian Sea into Indian subcontinent has provided the favourable conditions for
372 occurrence of extreme precipitation events (e.g., Priya et al. 2017). There are significant differences
373 in LLJ spatial structure and had a broader LLJ during extreme event compared before and after the
374 event (Figure 9). There have been many studies on heavy rainfall associated with increasing the
375 low-level winds over different parts of world (e.g., Chen and Li 1995; Takahasi 2004; Lima et al.
376 2009; Priya et al. 2017; Velloer et al. 2016; Xavier et al. 2018) as observed in the present case.

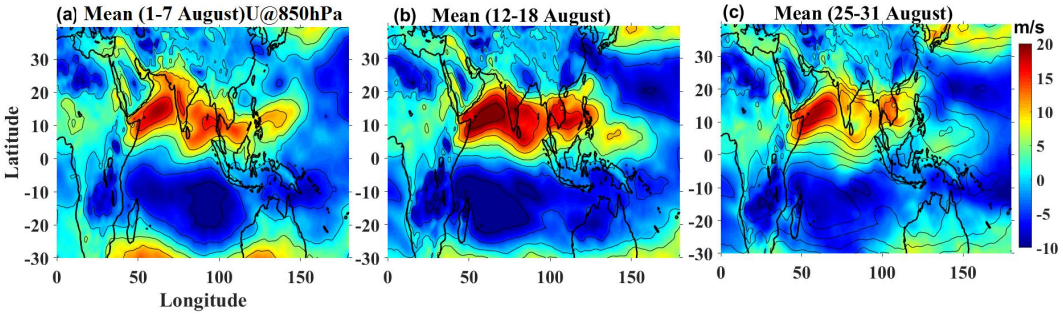

377

378 *Figure 9(a-c): The mean LLJ for three periods before (1st -7th August), during (12th -18th August)*
379 *and after (25th -31st August) respectively at 850 hPa.*
380

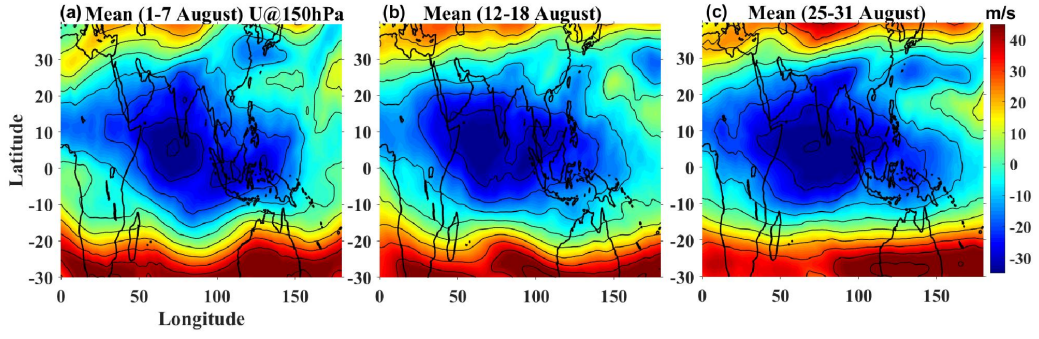

381

382 *Figure 10: Same as figure 9 but for TEJ at 150 hPa.*
383

384 We further examined the upper level changes in wind before, during and after the extreme event.
385 Figure 10 shows the mean upper tropospheric wind at 150 hpa (hereafter referred as TEJ) from (a)

https://doi.org/10.5194/nhess-2020-2
Preprint. Discussion started: 16 March 2020

Natural Hazards and Earth System Sciences
Discussions

386 1st -7th, (b) 12th -18th and (c) 25th -31st of August 2018 respectively over the Indian region. During
387 extreme precipitation period, the westerlies over the study region observed to be weakening and
388 further split into two as seen in Figure 10(b). Otherwise, the prevailed westerlies at 150 hPa were to
389 be strong as seen Figure 10 (a) and (c). The weakening of TEJ reduces the shear between the lower
390 troposphere and upper troposphere, which further favours the vertical development of convective
391 clouds as observed in spatial and vertical structure of precipitating cloud measured by C-band DWR
392 (Figure 4 and 5). Thus the present results indicate that the extreme precipitation event was mainly
393 influenced by large-scale atmospheric circulation. Chen and Li (1995) and Milrad et al. (2015) also
394 noted the changes in large-scale conditions were responsible for the genesis of heavy rainfall. In
395 modelling study by Kumar et al. (2008) also analysed the heavy rainfall event took place on 26th
396 July 2005 in Mumbai and found that the large-scale wind circulation motions are primary
397 responsible for the heavy rainfall using Weather Research Forecast model output. The changes in
398 meridional temperature gradient is primary responsible for the observed weakening of TEJ strength.

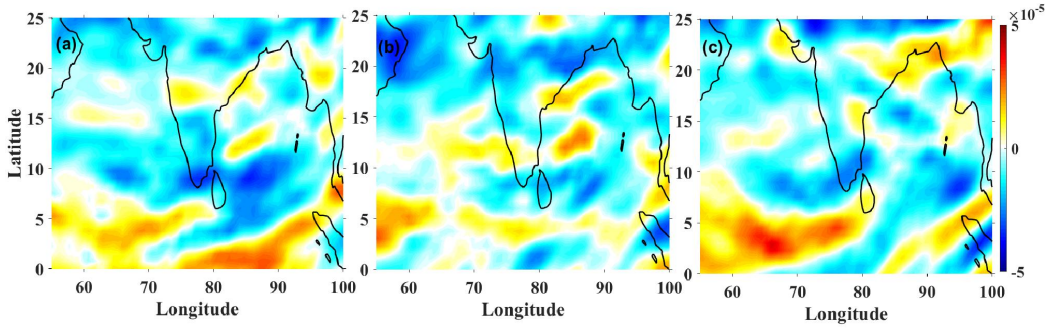

399

400 *Figure 11: Same as figure 9 but for divergence at 200 hPa.*
401

402 Figure 11 shows same as figure 9, but for divergence at 200 hPa. From this picture, it was found
403 that the divergence existed during the extreme precipitation period (Figure 11(b)) only, which is
404 associated with the low level convergence and helps to the development of convection. We also
405 examined the latitudinal (5^0-15^0 N) mean longitude–height structure of Omega (ω) over the study
406 region is shown in Figure 12, which is same as Figure 9. Negative (positive) values of Omega
407 indicate ascending (descending) motion (Figure 12(b)) between 70^0-80^0 E longitude bands. Strong

https://doi.org/10.5194/nhess-2020-2
Preprint. Discussion started: 16 March 2020

Natural Hazards and Earth System Sciences
Discussions

ascending was noticed from surface to 10 km height, which associated with the very intense precipitation. Associated descending motion also enhanced during intense rainfall compared to before and after as seen in Figure 12(a) & (c). Figure 13 shows same as figure 9, but for vertical profile of temperature. There clear enhancement in vertical column of temperature almost throughout troposphere during extreme event (red colour) compared to non-extreme period (black and blue colour lines). The difference in temperature during and after was plotted in Figure 13(b). It was found that difference in temperature around 2K from mid-troposphere (~ 4 km) to upper troposphere (~15 km), which further fuels the development of vigorous convection as led to the extreme precipitation. This difference mainly due to the latent heating of condensation and the shape of temperature difference profile looks like a latent heating structure in deep convective system with dominant stratiform region. Further, the release of latent heating during heavy precipitation strongly influences the atmospheric circulation and feedback. The evaporative cooling in extreme precipitation causes the negative difference in temperature at lower level (below 4km).

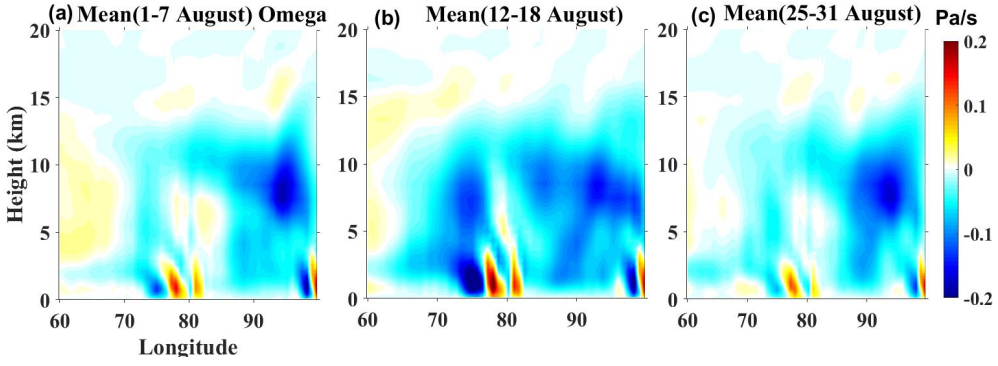

Figure 12: same as figure 9 but for the latitudinal (5^0-15^0 N) mean longitude–height structure of Omega (ω).

https://doi.org/10.5194/nhess-2020-2
Preprint. Discussion started: 16 March 2020

Natural Hazards and Earth System Sciences
Discussions

20

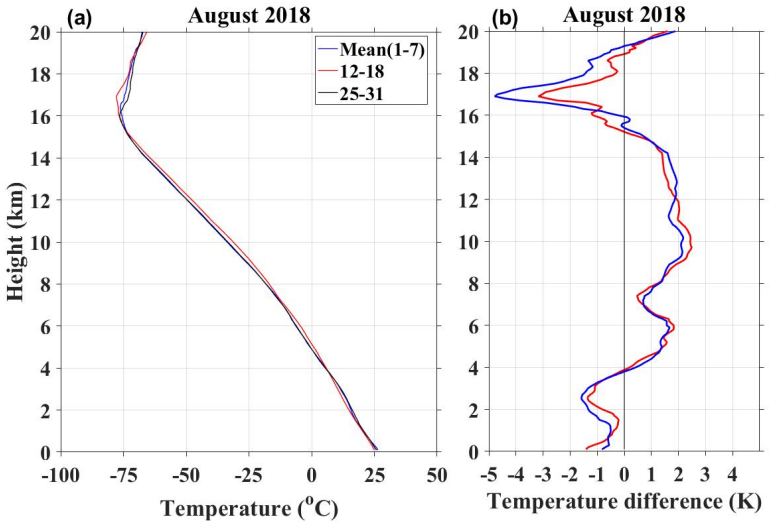

425

426 *Figure 13: (a) same as figure 9 but for Temperature profile (b) temperature difference between*
427 *during and before (blue color) and during and after (red color).*
428
429
430 There have been few studies related extreme events to equatorially trapped waves, especially Kelvin
431 and Rossby waves (e.g., Wheeler et al. 2000; Takahasi 2004). We also investigated the presence of
432 such type of waves during extreme events. The daily wind speed anomalies over the study region at
433 150 hPa are subjected to wavelet analysis and extracted the period and amplitudes, which are
434 plotted in Figure 14. Interestingly, westward equatorial waves were present in the period of 7-10
435 days throughout the month of August. But their amplitude became weaken just before the extreme
436 event and continue to be weakened as seen in Figure 14. Wheeler et al. (2000) also found the
437 similar period of waves in zonal wind during heavy rainfall event and confirmed that these are
438 convectively coupled equatorial waves (Kelvin and Rossby) in the troposphere. Another study by
439 Takahasi (2004) also documented that presence of these waves. Very recently, Ferret et al. (2019)
440 found that the presence the probability of extreme precipitation is dependent on equatorial wave
441 activity and heavy precipitation can be up to three times more likely in regions of South East Asia
442 during the presence of equatorial waves (Ferret et al., 2019). The weakening of equatorial waves
443 just before the extreme event might have caused for the observed divergence at upper level as seen
444 in Figure 11.Thus the present findings suggest that the combined effect of strengthened southwest

https://doi.org/10.5194/nhess-2020-2
Preprint. Discussion started: 16 March 2020

Natural Hazards and Earth System Sciences
Discussions

445 monsoon circulation, weakened westerlies at upper levels and the presence of strong updrafts were
446 provided the favourable conditions for the observed extreme precipitation event took place in
447 August 2018 over Kerala.

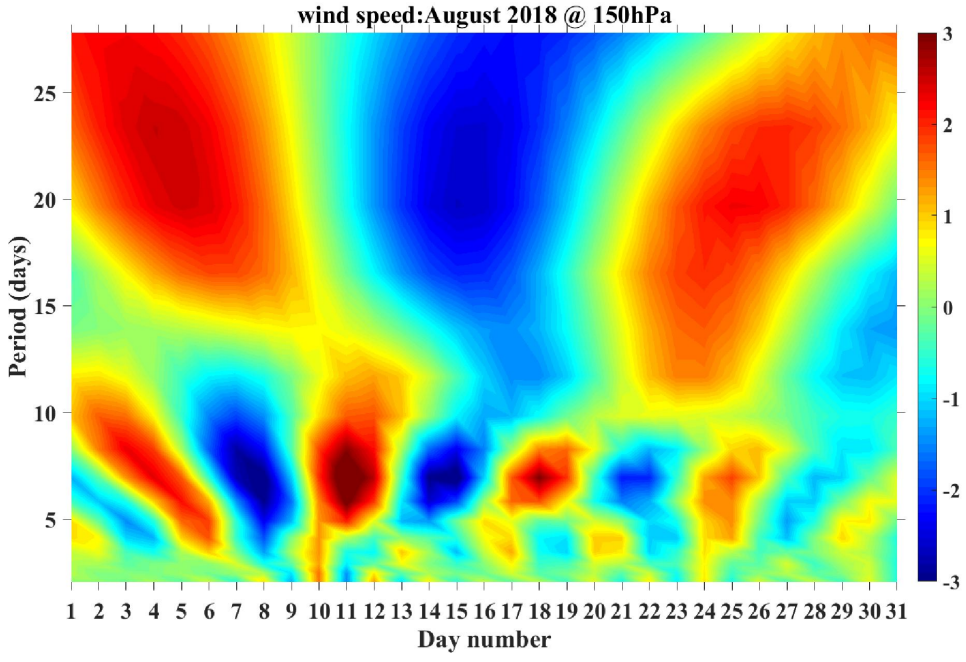

448

449 *Figure 14: Wavelet analysis for wind speed at 150 hPa on 15th August 2018.*
450
451
452 **4. Summary and conclusion**

453

454 The present paper investigated the spatial and vertical structure of precipitating clouds during recent
455 extreme precipitation event in Kerala using C-band polarimetric DWR observations at Thumba and
456 the role of large-scale circulations were examined. DWR observations showed that there are
457 multiple shallow convective cells behind the leading convective cell, which were embedded in the
458 frontal convective system and whose cloud tops are 10 km and above. The maximum reflectivity
459 and width of convective core found to be 45 dBZ and 7 km respectively. The rapid development of
460 precipitation took during first intense spell in which increased rain intensity as well as wide spatial
461 pattern was observed. The most of the hydrometeor particles are oriented in horizontal direction and

https://doi.org/10.5194/nhess-2020-2
Preprint. Discussion started: 16 March 2020

Natural Hazards and Earth System Sciences
Discussions

462 oblate in shape, where the maximum Z_{dr} found to be 0.8 to 1 dB. It was found that firstly, the
463 atmosphere as fully saturated up to 400 hPa and has the very high CAPE which has favourable
464 conditions for moist convective instability to initiate occurrence of convection. It was also found
465 that strengthening of LLJ at lower level provided the surplus moisture and weakening of TEJ at
466 upper levels decrease of vertical shear, which favours the vertical development of convective
467 clouds. It was found that the weakening of equatorial waves (~7-10 days) during the extreme period
468 and might have caused the observed upper level divergence associated with low level convergence,
469 which helped to the development of convection. Thus, the present results suggest that the combined
470 effects of LLJ, TEJ and the presence of equatorial waves along with the presence of strong updrafts
471 were caused the occurrence of extreme precipitation. These results are summarized schematically in
472 Figure 15, which provided an overview of changes in background dynamics before and during the
473 extreme precipitation event. Hence, the significance of the present study lies in demonstrating the
474 role of atmospheric dynamics for the spatial and vertical structure of precipitating cloud observed
475 by c-band DWR during extreme precipitation event, which will be useful in understanding and
476 modelling the role of atmospheric circulation in extreme events.
477

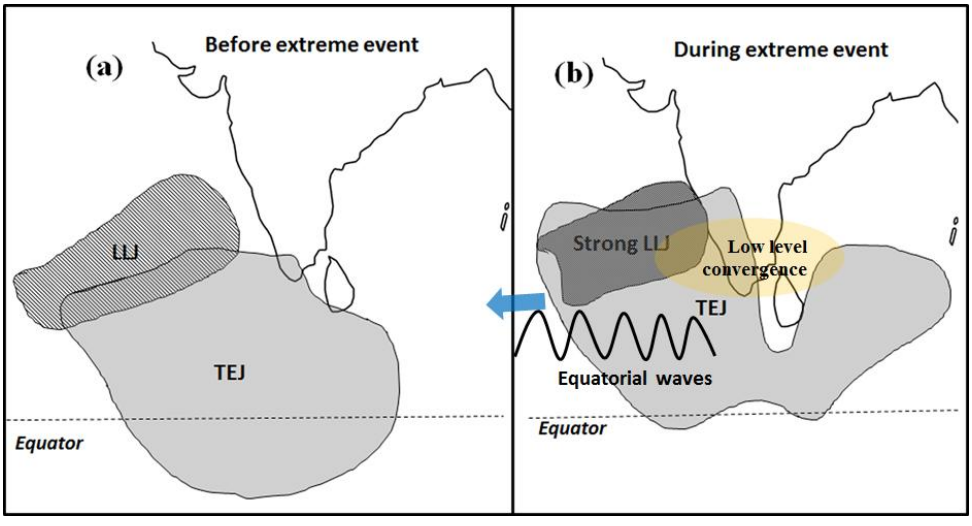

478

479 *Figure 15. Overview of changes in large-scale circulations such as spatial structure of LLJ and TEJ*
480 *before and during the extreme precipitation event.*

https://doi.org/10.5194/nhess-2020-2
Preprint. Discussion started: 16 March 2020

Natural Hazards and Earth System Sciences Discussions

481
482 **Acknowledgements**

483

484 The soundings over Trivandrum were obtained from University of Wyoming
485 http://weather.uwyo.edu/upperair/sounding.html. The authors thank to Era-Interim reanalysis team
486 for providing the reanalysis winds data publically. The authors thank to DGM, TERLS and those
487 who supported the continuous operation of DWR. We thank to Director, SPL for constant support
488 and encouragement for carrying out this study.

489
490
491 **References**

492 Ajayamohan, R. S., Merryfield, W. J., and Kharin, V. V.: Increasing trend of synoptic activity and
493 its relationship with extreme rain events over central India, J. Clim., 23,1004-1013, 2010.

494 Alcide, D. Z., Stevenson, D. S., and Bollasina, M. A.: The role of anthropogenic aerosols in future
495 precipitation extremes over the Asian Monsoon Region, Clim. Dyn.,
496 https://doi.org/10.1007/s00382-018-4514-7, 2019.

497 Alexander, L. V. et al.: Global observed changes in daily climate extremes of temperature and
498 precipitation, J. Geophys. Res., 111:D05109, 2006.

499 Allen, M. R., and Ingram, W. J.: Constraints on future changes in climate and the hydrologic cycle,
500 Nature, 419: 224–232, 2002.

501 Kumar, A. D., Rotunno, R., Niyogi, D., and Mohanty, U. C.: Analysis of the 26 July 2005 heavy
502 rain event over Mumbai, India using the Weather Research and Forecasting (WRF) model, Q. J.
503 Royal Meteorol. Soc., 134: 1897–1910, 2008

https://doi.org/10.5194/nhess-2020-2
Preprint. Discussion started: 16 March 2020

Natural Hazards and Earth System Sciences Discussions

504 Xavier, A., Manoj, M. G., and Mohankumar, K.: On the dynamics of an extreme rainfall event in
505 northern India in 2013, J. Earth Syst. Sci., 127:30, https://doi.org/10.1007/s12040-018-0931-6,
506 2018.

507 Catto, J. L., Jakob, C., Berry, G., and Nicholls, N.: Relating global precipitation to atmospheric
508 fronts, Geophys. Res. Lett., 39, L10805. https ://doi.org/10.1029/2012GL051736, 2012.

509 Catto, J. L., and Pfahl, S.: The importance of fronts for extreme precipitation, J. Geophys. Res., 118,
510 10,791–10, 801. https://doi.org/10.1002/jgrd.50852, 2013

511 Chen, C. Y., Chen, Y. L., Chen, C. S., Lin, P. L., and Liu, C. L.: Revisiting the heavy rainfall event
512 over northern Taiwan on 3 June 1984, Terr. Atmos. Ocean. Sci., 24, 999-1020,
513 doi:10.3319/TAO.2013.07.04.01 (A), 2013

514 Chen, Y. L., and Li, J.: Large scale Conditions favorable for the development of heavy rainfall
515 during TAMEX IOP 3, Mon. Wea. Rev., 123, 1995.

516 Collow, A. B. M., Bosilovich, M. G., and Koster, R. D.: Large-scale influences on summertime
517 extreme precipitation in the northeastern United States, J. Hydrometeorol., 17, 3045–3061. https
518 ://doi. org/10.1175/jhm-d-16-0091.1, 2016

519 Del Genio, A. D., and Kovari, W.: Climatic Properties of Tropical Precipitating Convection under
520 Varying Environmental Conditions, J. Clim., 15, 2597–2615, 2002.

521 Derbyshire, S. H. et al.: Sensitivity of moist convection to environmental humidity, Q. J. Royal
522 Meteorol. Soc., 130, 3055–3079, 2004.

523 Ding, Y.: The variability of the Asian summer monsoon. In: Kluwer Academic, editor. Monsoon
524 over China, J. Meteor. Soc. Japan., 85B, 21-54. DOI: 10.2151/jmsj.85B. 21, 1994

https://doi.org/10.5194/nhess-2020-2
Preprint. Discussion started: 16 March 2020

525 Ding, Y.: The variability of the Asian summer monsoon, J. Meteor. Soc. Japan., 85B, 21-54. DOI:
526 10.2151/jmsj.85B.21, 2007

527 Ding, Y., and Sikka, D. R.: In The Asian Monsoon, Springer Berlin Heidelberg, 131–201,
528 https://doi.org/10.1007/3-540-37722-0-4, 2006.

529 Feng, Z. et al.: Life cycle of midlatitude deep convective systems in a Lagrangian framework, J.
530 Geophys. Res., 117, 2012.

531 Goswami, B. N., Venugopal, V., Sengupta, D., Madhusoodanan, M. S., and Xavier, P. K.:
532 Increasing trend of extreme rain events over India in a warming environment, Science, 314,1442-
533 1445, 2006

534 Grossman, R. L., and Durran, D. R.: Interaction of low-level flow with the Western Ghat Mountains
535 and offshore convection in the summer monsoon, Mon. Wea. Rev., 112, 652–672, 1984.

536 Held, I., and Soden, B.: Robust responses of the hydrological cycle to global warming, J. Clim., 19,
537 5686–5699, 2006

538 Hennessey, K. J., Gregory, J. M., and Mitchell, J. F. B.: Changes in daily precipitation under
539 enhanced greenhouse conditions, Clim. Dyn., 13, 667–680, 1997.

540 Herring, S. C., Hoerling, M. P., Peterson, T. C., and Stott, P. A. Eds.: Explaining Extreme Events of
541 2013 from a Climate Perspective, Bull. Amer. Meteor. Soc., 95 (9), S1–S96, 2014.

542 Baisya, H., Pattnaik, S., Hazra, V., Sisodiya, A., and Rai, D.: Ramifications of Atmospheric
543 Humidity on Monsoon Depressions over the Indian Subcontinent, Scientific report,
544 DOI:10.1038/s41598-018-28365-2, 2018.

https://doi.org/10.5194/nhess-2020-2
Preprint. Discussion started: 16 March 2020

Natural Hazards and Earth System Sciences Discussions

545 Houze, R. A., Rasmussen, K. L., Medina, S., Brodzik, S. R., and Romatschke, U.: Anomalous
546 Atmospheric events leading to the summer 2010 floods in Pakistan, Bull. Amer. Meteor. Soc., DOI:
547 10.1175/2010BAMS3173.I, 2011.

548 Houze, R. A., Chen, S. S., Lee, W. C., Rogers, R. F., Moore, J. A., Stossmeister, G.J., Bell, M.M.,
549 Cetrone, J.L., Zhao, W., and Brodzik, S.R.: The Hurricane Rainband and Intensity Experiment:
550 Observations and modeling of Hurricanes Katrina, Ophelia, and Rita, Bull. Amer. Meteor. Soc., 87,
551 1503-1521, 2006.

552 Nie, J., Sobel, A. H., Shaevitz, D. A., and Wang, S.: Dynamic amplification of extreme precipitation
553 sensitivity, Proceedings of the National Academy of Sciences of the United States of America,
554 doi/10.1073/pnas.1800357115, 2018.

555 Takahashi, K.: The atmospheric circulation associated with extreme rainfall events in Piura, Peru,
556 during the 1997–1998 and 2002 El Niño events, Anna. Geophys., 22, 3917–3926, 2004.

557 Kao, S. C., and Ganguly, A. R.: Intensity, duration, and frequency of precipitation extremes under
558 21st-century warming scenarios, J. Geophys. Res., 116, D16119, 2011

559 Kirsch, T. D., Wadhwani, C., Sauer, L., Doocy, S., and Catlett, C.: Impact of the 2010 Pakistan
560 floods on rural and urban populations at six months, PLOS Currents,
561 https://doi.org/10.1371/4fdfb212d2432, 2012.

562 Agel, L., Barlow, M., Colby, F., Binder, H., Catto, J. L., Hoell, A., and Cohen, J.: Dynamical
563 analysis of extreme precipitation in the US northeast based on large-scale meteorological patterns,
564 Clim. Dyn., https://doi.org/10.1007/s00382-018-4223-2, 2018.

565 Lima, K. C., Satyamurty, P., and Fernandez, J. P. R.: Large scale atmospheric conditions associated
566 with heavy rainfall episodes in Southeast Brazil, Theor. Appl. Climatol., DOI, 10.1007/s00704-009-
567 0207-9, 2009.

https://doi.org/10.5194/nhess-2020-2
Preprint. Discussion started: 16 March 2020

Natural Hazards and Earth System Sciences Discussions

568 Milrad, S. M., Gyakum, J. R., and Atallah, E. H.: A meteorological analysis of the 2013 Alberta
569 flood: Antecedent large-scale flow pattern and synoptic-dynamic characteristics, Mon. Wea. Rev.,
570 143, 2817–2841, https://doi.org/10.1175/MWR-D-14-00236.1, 2015.

571 Muller, et al.: Intensification of Precipitation Extremes with Warming in a Cloud-Resolving Model,
572 J. Clim., 2011.

573 O'Gorman, P. A.: Precipitation extremes under climate change, Current Climate Change Reports, 1,
574 49–59, https://doi.org/10.1007/s40641-015-0009-3, 2015.

575 O'Gorman, P. A., and Schneider, T.: Scaling of precipitation extremes over a wide range of climates
576 simulated with an idealized GCM, J. Clim., 22, 5676–5685.
577 https://doi.org/10.1175/2009JCLI2701.1, 2009a

578 O'Gorman, P. A., and Schneider, T.: The physical basis for increases in precipitation extremes in
579 simulations of 21st-century climate change, Proceedings of the National Academy of Sciences of
580 the United States of America, 106, 14773–14777, 2009b.

581 Pall, P., Allen, M. R., and Stone, D. A.: Testing the Clausius- Clapeyron constraint on changes in
582 extreme precipitation under CO 2 warming, Clim. Dyn., 28, 351–363, 2007.

583 Pfahl, S., O'Gorman, P. A., and Fischer, E. M.: Understanding the regional pattern of projected
584 future changes in extreme precipitation, Nature Climate Change, 7, 423–427.
585 https://doi.org/10.1038/nclimate3287, 2017.

586 Priya, P., Krishnan, R., Mujumdar, M., and Houze, R. A.: Changing monsoon and midlatitude
587 circulation interactions over the Western Himalayas and possible links to occurrences of extreme
588 precipitation, Clim. Dyn., 49, 2351. https://doi.org/10.1007/s00382-016-3458-z, 2017.

https://doi.org/10.5194/nhess-2020-2
Preprint. Discussion started: 16 March 2020


Natural Hazards and Earth System Sciences Discussions

589 Rajeevan, M., Bhate, J., and Jaswal, A. K.: Analysis of variability and trends of extreme rainfall
590 events over India using 104 years of gridded daily rainfall data, Geophys. Res. Lett., 35, L18707,
591 doi:10.1029/2008GL035143, 2008.

592 Rajendra Kumar, J., and Dash, S. K.: Interdecadal variations of characteristics of monsoon
593 disturbances and their epochal relationships with rainfall and other tropical features, Int. J.
594 Climatol., 21, 759-771, 2001.

595 Sarker, R. P.: Some modifications in a dynamical model of orographic rainfall, Mon. Wea. Rev., 95,
596 673–684, 1967.

597 Schumacher, R. S.: Floods, Convective Storms. Encyclopedia of Natural Hazard Science, Heavy
598 Rainfall and Flash Flooding, DOI: 10.1093/acrefore/9780199389407.013.132, 2017.

599 Sherwood, S.C., et al.: Relative humidity changes in a warmer climate, J. Geophys. Res., 115,
600 D09104, 2010.

601 Shi, X., and Durran, D. R.: Estimating the response of extreme precipitation over mid-latitude
602 mountains to global warming, J. Climate, doi: 10.1175/JCLI-D-14-00750.1, 2015.

603 Siler, N., and Roe, G.: How will orographic precipitation respond to surface warming? An idealized
604 thermodynamic perspective, Geophys. Res. Lett., 41, 2606–2613., 2014.

605 Soden, B. J., and Held, I. M.: An Assessment of Climate Feedbacks in Coupled Ocean–Atmosphere
606 Models, J. Clim., 19, 3354–3360, 2006.

607 Tandon, N. F., Zhang, X., and Sobel, A. H.: Understanding the dynamics of future changes in
608 extreme precipitation intensity, Geophys. Res. Lett., 45, 2870–2878.
609 https://doi.org/10.1002/2017GL076361, 2018.

https://doi.org/10.5194/nhess-2020-2
Preprint. Discussion started: 16 March 2020

Natural Hazards and Earth System Sciences Discussions

610 Trenberth, K. E.: Conceptual framework for changes of extremes of the hydrological cycle with
611 climate change, Climatic Change, 42, 327–339, 1999.

612 Dayan, U., Nissen, K., and Ulbrich, U.: Review Article: Atmospheric conditions inducing extreme
613 precipitation over the eastern and western Mediterranean, Nat. Hazards Earth Syst. Sci., 15, 2525–
614 2544, doi:10.5194/nhess-15-2525-2015, 2015.

615 Krishnamurthy, V.: Extreme Events and Trends in the Indian Summer Monsoon, COLA Technical
616 Report 314, 2011.

617 Mishra, V., Aadhar, S., Shah, H, and Kumar, R.: Dushmanta Ranjan Pattanaik, Amar Deep Tiwari,
618 The Kerala flood of 2018: combined impact of extreme rainfall and reservoir storage, Hydrol.
619 Earth. Syst. Sci. Discuss., https://doi.org/10.5194/hess-2018-480, 2018.

620 Wang, B.: The Asian Monsoon. Praxis Publishing, Chichester, UK. 787 p., 2006.

621 Westra, S., Alexander, L.V., and Zwiers, F. W.: Global increasing trends in annual maximum daily
622 precipitation, J. Clim., 26, 3904–3918, 2013.

623 Zhao, A. D., Stevenson, D. S., and Bollasina, M. A.: The role of anthropogenic aerosols in future
624 precipitation extremes over the Asian Monsoon Region. Clim Dyna, DOI: 10.1007/s00382-018-
625 4514-7, 2018.

626
627

628